Supplementary Information (SI) for Journal of Materials Chemistry A.
This journal is © The Royal Society of Chemistry 2025

Dynamic Coupling Mechanism in $NbSe_2/MoSe_2$ Heterojunctions for Enhanced Temperature Adaptability of Lithium-Ion Batteries

Lingfeng Zhang[a], Zihao Li[a], Liying Wang[a], Xijia Yang[a], Yue yang[a], Yang Gao[a], Xiaohan Zhang[a], Xuesong Li[a*], Wei Lü[a,b,c*]

[a]Key Laboratory of Advanced Structural Materials, Ministry of Education and School of Materials Science and Engineering, Changchun University of Technology, Changchun 130012, China

[b]Advanced Institute of Materials Science, Changchun University of Technology, Changchun 130012, China

[c]State Key Laboratory of Luminescence Science and Technology, Changchun Institute of Optics, Fine Mechanics and Physics, Chinese Academy of Sciences, Changchun 130033, China

E-mail: lw771119@hotmail.com, lixuesong@ccut.edu.cn

Fax: +86-0431-85716426; Tel: +86-0431-85716421

* To whom all correspondence should be addressed.

1．Experiment section

1.1．Synthesis of $NbSe_2/MoSe_2$

Dissolve 0.1 mmol of $(NH_4)_6Mo_7O_{24}·4H_2O$ and 0.1 mmol of $NbCl_5$ separately in 30 mL of deionized water and 20 mL of ethanol, respectively, stirring until fully dissolved. After mixing the resulting solutions and stirring thoroughly, transfer the mixed solution to a 50 mL reaction vessel lined with PTFE (Teflon) and heat at 160 ℃ for 24 h. Wash the obtained product three times with deionized water and anhydrous ethanol, then dry at 60 ℃ for 24 h to obtain a deep blue powder precursor.

$MoSe_2/NbSe_2$ gray powder was obtained by annealing a mixture of the precursors and NaCl with Se powder in a ceramic boat (mass ratio 1 :1.2 :1.5) at 900 °C for 5 h under a flowing Ar/H_2 gas mixture in a tube furnace.

Synthesis of $MoSe_2$

Dissolve 0.1 mmol of $(NH_4)_6Mo_7O_{24}·4H_2O$ in a mixed solution of 30 mL deionized water and 20 mL ethanol, stirring until fully dissolved. Transfer the resulting solution to a 50 mL reaction vessel lined with PTFE (Teflon) and heat at 160 ℃ for 24 h. Wash the obtained product three times with deionized water and anhydrous ethanol, then dry at 60 ℃ for 24 h to obtain a brown powder precursor.

Place the precursor , NaCl, and selenium powder into a ceramic boat, and anneal in a tube furnace at 900 ℃ under a mixed argon-hydrogen gas flow for 5 h to obtain $MoSe_2$ powder.

1.2．Material characterization

The phases and composition were characterized by X-ray diffraction (XRD, SmartLab9KW with Cu-Kα radiation at 40 kV, λ = 1.541 Å), X-ray photoelectron spectroscopy (XPS, Escalab 250Xi), Raman spectroscopy (Renishaw InVia, 532 nm excitation wavelength) and energy-dispersive spectroscopy (EDS, FEI Talos F200S). The microstructures and morphology were investigated through field-emission scanning electron microscopy (FESEM, Thermo Fisher Scientific Apreo C, USA) and transmission electron microscopy (TEM, Talos F200S, FEI, Thermo). The specific surface area and pore size distribution (PSD) were analyzed by the Brunauer-Emmett-Teller method (BET, Micromeritics ASAP2460) and the Barrett-Joyner-Halenda (BJH) method, respectively.

1.3. Electrochemical test

The working electrode was prepared by mixing the active material ($NbSe_2$/$MoSe_2$), sodium carboxymethyl cellulose (CMC), and conductive carbon black in a weight ratio of 8:1:1 with deionized water as the solvent. The slurry was uniformly coated onto a copper foil, which was then dried in an oven at 60 ℃ for 2 h and further vacuum-dried at 80 ℃ for 12 h. After drying, the copper foil was punched into 12 mm discs, with an average loading of 1.2-1.6 mg cm^{-2}. CR2025 coin-type half-cells were assembled in a glove box filled with Ar, where the H_2O and O_2 content was below 0.01 ppm. The separator used was a single-layer polypropylene membrane (Celgard, 2500). The electrolytes used were: (1) 1M $LiPF_6$ in DMC:EC:EMC = 1:1:1 Vol% with 10% FEC, (2)1M $LiPF_6$ in DEC:EC:EMC = 1:1:1 Vol% with 10% FEC.

Cyclic voltammetry (CV) measurements were performed on an electrochemical workstation (CHI660E) at a scan rate of 0.1 mV s^{-1}. Electrochemical impedance spectroscopy (EIS) was conducted on the same workstation (CHI660E) in the frequency range of 0.01 Hz to 1×10^5 Hz. The constant current charge/discharge tests were carried out on a LANHE battery testing system (CT-3002A, Wuhan, China). All specific capacity values are based on the mass of $MoSe_2/NbSe_2$. The rate and high-current half-cell tests were conducted using cells that had undergone 10 pre-cycles. For tests at -25 ℃, the cells were pre-activated with 3 cycles at room temperature before testing.

1.4. Analog calculation

The theoretical calculations involved in this study were performed using simulation software. First, the molecular models were constructed using the simulation software. Then, the DMol3 module was used to optimize the geometries of different molecular models. The structural and electronic properties of $MoSe_2/NbSe_2$ and $MoSe_2$ were calculated using the simulation software. The calculations were based on density functional theory (DFT) with the Generalized Gradient Approximation (GGA) and the Perdew-Burke-Ernzerhof (PBE) functional for handling exchange and correlation terms. The wavefunction was truncated at 550 eV, and the energy convergence criterion was set to 10^{-6} eV. A 2×2×2 mesh was used for Li point sampling. To avoid interactions, a vacuum layer of 15 Å was placed around the $MoSe_2/NbSe_2$ composite and $MoSe_2$ in the simulation model. The Castep module was used to evaluate the structural and electronic properties of $MoSe_2/NbSe_2$ and $MoSe_2$, as well as the adsorption energy and

work function of $MoSe_2$/$NbSe_2$ and $MoSe_2$ for Li^+. To study the movement of Li^+ in the composite, molecular dynamics calculations and analysis were performed using the Forcite module. The radial distribution function (RDF) was obtained from the MD simulation results, and the coordination number of sodium ions was calculated.

1.5. Full battery test

The $LiFePO_4$cathode material was tested in a half-cell configuration. Figure R11 shows the voltage-specific capacity profile of the half-cell during the third cycle, with a discharge specific capacity of 153 mAh g^{-1}. The cathode was prepared using an Al foil current collector with a diameter of 12 mm, yielding an active material loading of about 3.4 mg cm^{-2} and an areal capacity of approximately 0.52 mAh cm^{-2}.

The $NbSe_2$/$MoSe_2$ anode fabricated in this work delivered a reversible charge specific capacity of ~586.6 mAh g^{-1} in the third cycle under the corresponding test current density. The anode was prepared on a Cu foil current collector with a diameter of 16 mm, giving an active material loading of about 1.05 mg cm^{-2} and an areal capacity of ~0.624 mAh cm^{-2}. The NP ratio is calculated as:

$$NP = \frac{Anode\_sc \times Anode\_td \times Anode\_amcr}{Cathode\_sc \times Cathode\_td \times Cathode\_amcr}$$

In this equation:

1.Anode_sc is Anode specific capacity.

2. Anode_td is Anode tap density.

3. Anode_amcr is Anode active material content ratio.

4. Cathode_sc is Anode specific capacity.

5. Cathode_td is Anode tap density.

6. Cathode_amcr is Anode active material content ratio.

Based on the formula, the NP ratio for the full cell is 1.2:1.

1.6 Calculation formula

Equation S1. $D = 4/\pi\tau\,(mV_m/MA)^2(\Delta Es/\Delta E\tau)^2$. Where, τ represents the relaxation time, m denotes the mass of the active material, V_m refers to the molar volume, A represents the surface area of the electrode, ΔEs is the steady-state voltage change in volts, and ΔE is the voltage change caused during constant current charge-discharge process in volts.

Equation S2. *i=avb and log i=b log v + log a.*

Equation S3. *Battery weight energy density = Battery capacity * Discharge platform/weight.*

Fquation S4. *The correction adsorption energy (ΔE_ads) of the lithium battery anode material is defined as:*

$$\Delta E_{ads} = (E_{total} - E_{host} - nE_{Li^+}) / n \qquad (1)$$

In this equation:

1. E_{total} is the total energy after the interaction between the battery anode material and Li^+.

2. Ehost is the energy of the anode material itself.

3. E Li^+ is the energy of the Li^+ ion.

4. (n) is the number of Li^+ ions involved, where in the following studies, (n=1) is used.

1.7 Electrochemical equation

Reaction S1. The electrochemical reaction during the lithium storage of $MoSe_2$/$NbSe_2$

is as follows:

$$MoSe_2 + Li^+ + xe^- \rightleftharpoons Li_xMoSe_2 \quad (2)$$

$$NbSe_2 + Li^+ + xe^- \rightleftharpoons Li_xNbSe_2 \quad (3)$$

$$Li_xMoSe_2 + (4 - x)\ Li^+ + (4 - x)e^- \rightleftharpoons 2Li_2Se + Mo \quad (4)$$

$$Li_xNbSe_2 + (4 - x)\ Li^+ + (4 - x)e^- \rightleftharpoons 2Li_2Se + Nb \quad (5)$$

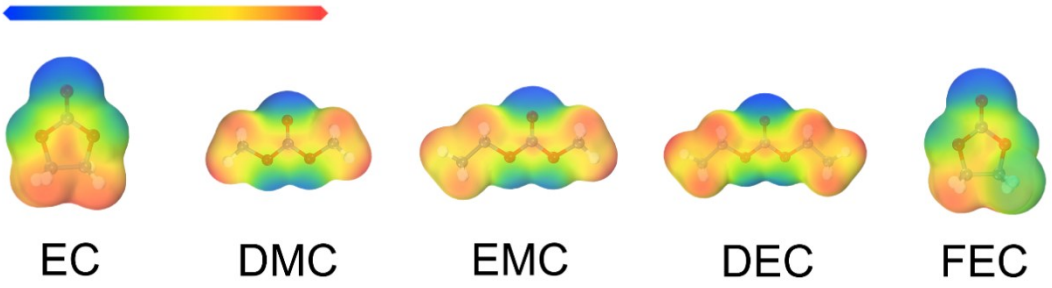

Fig. S1. The electrostatic potential of Li^+ with respect to EC, EMC, DMC, DEC, and FEC.

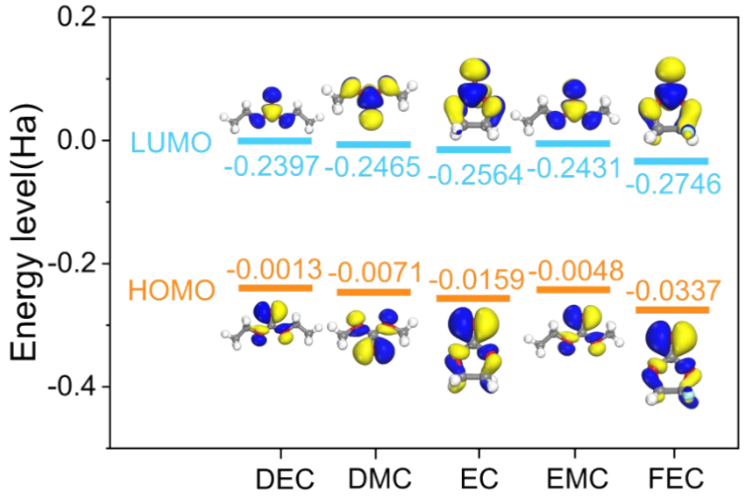

Fig. S2. The HOMO and LUMO energy levels of DEC, DMC, EC, EMC, and FEC.

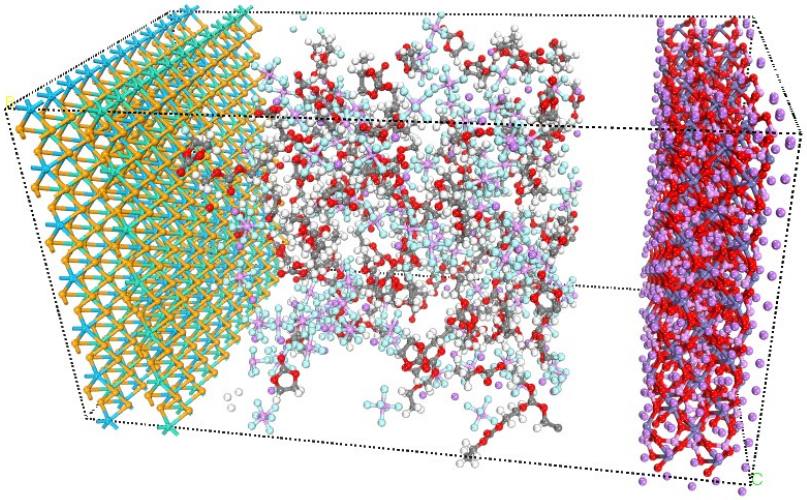

Fig. S3. $NbSe_2/MoSe_2$-EEM MD simulation snapshots.

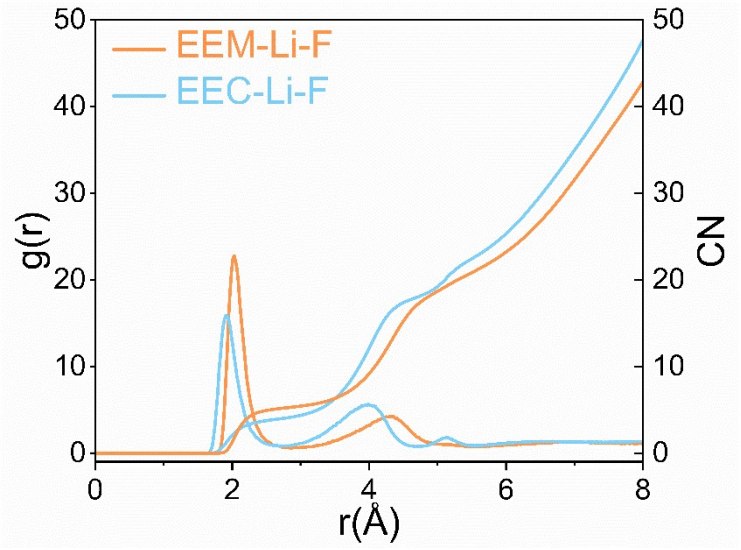

Fig. S4. Radial distribution function and coordination number of Li^+ and PF_6^-

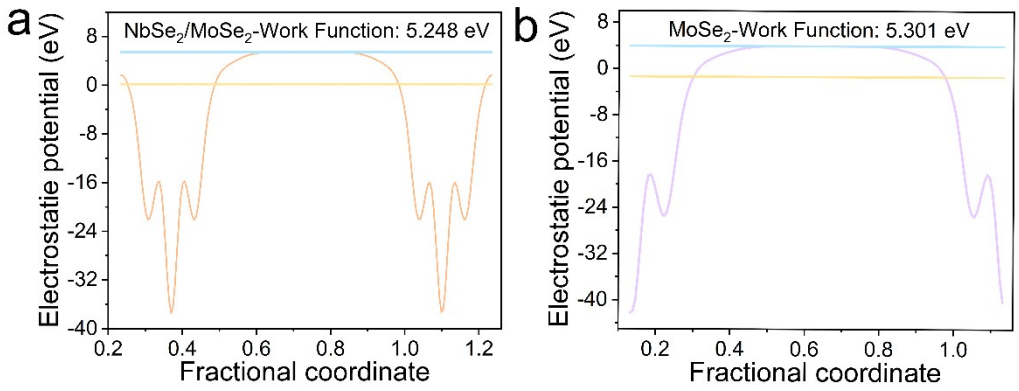

Fig. S5. Function of power of (a) $NbSe_2/MoSe_2$ and (b) $MoSe_2$.

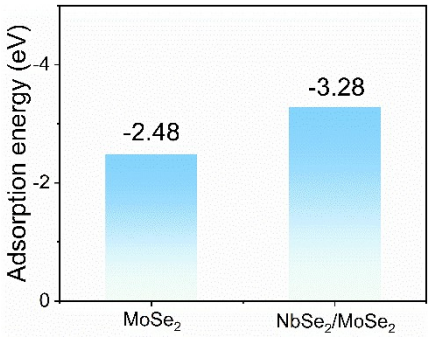

Fig. S6. Adsorption energy of $NbSe_2/MoSe_2$ and $MoSe_2$ for Li^+.

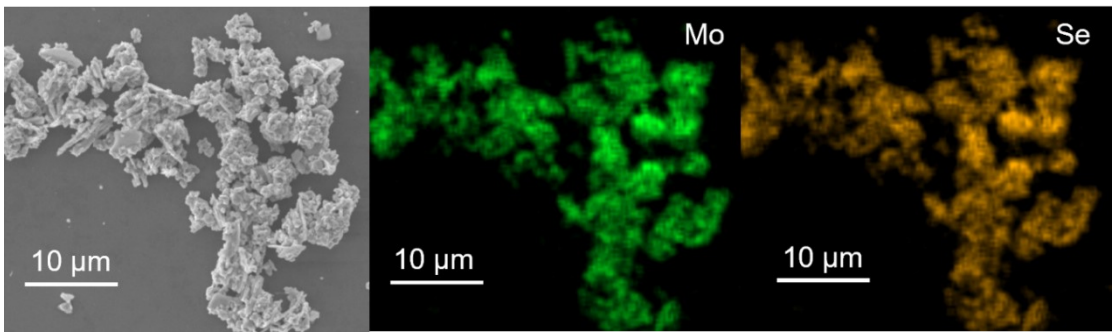

Fig. S7. EDS mappings of $MoSe_2$.

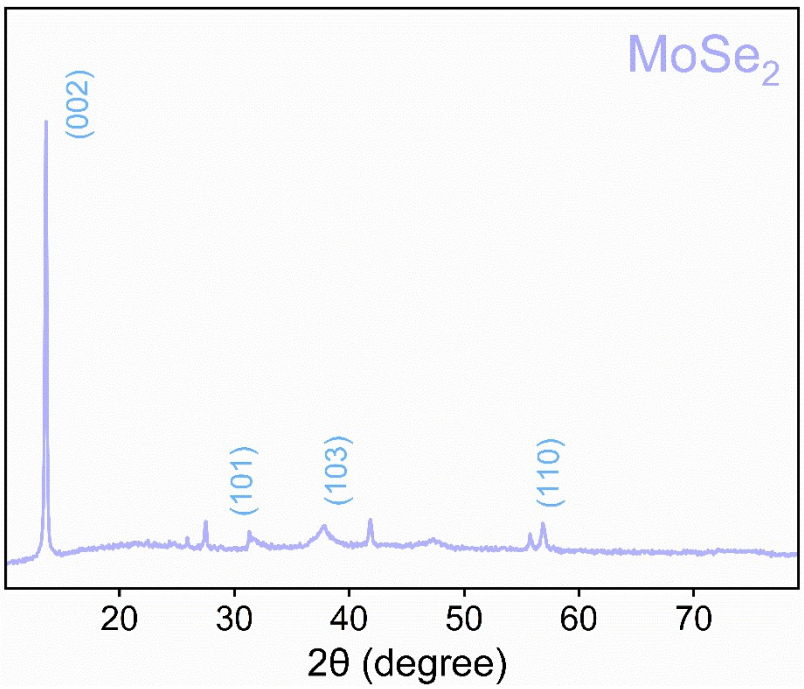

Fig. S8. XRD pattern of $MoSe_2$.

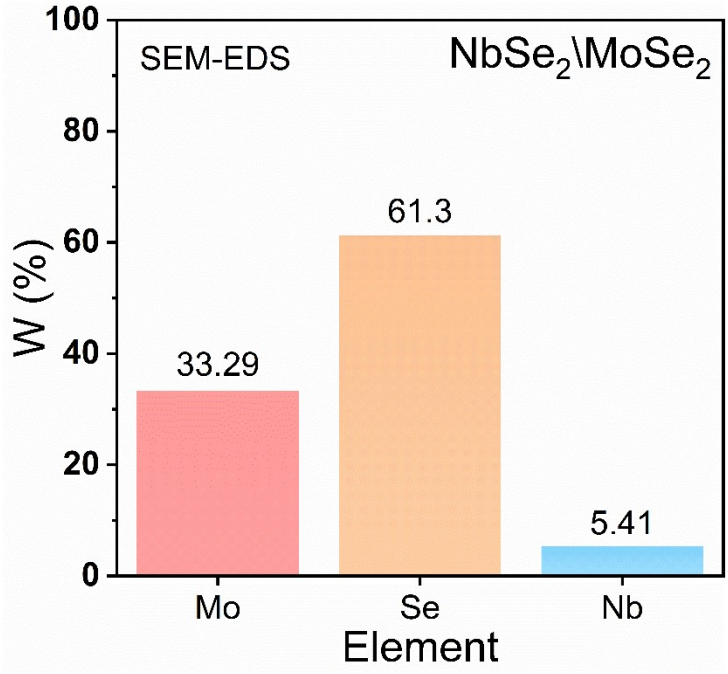

Fig. S9 Elemental composition of $NbSe_2$/$MoSe_2$ determined by SEM-EDS.

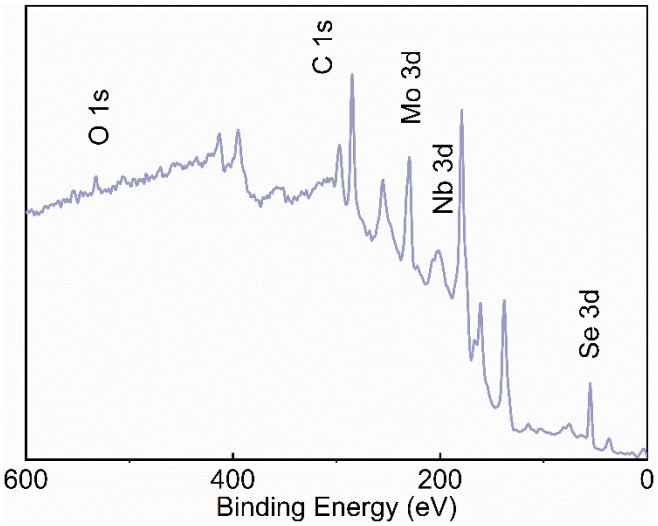

Fig. S10 XPS survey spectrum of the $NbSe_2/MoSe_2$

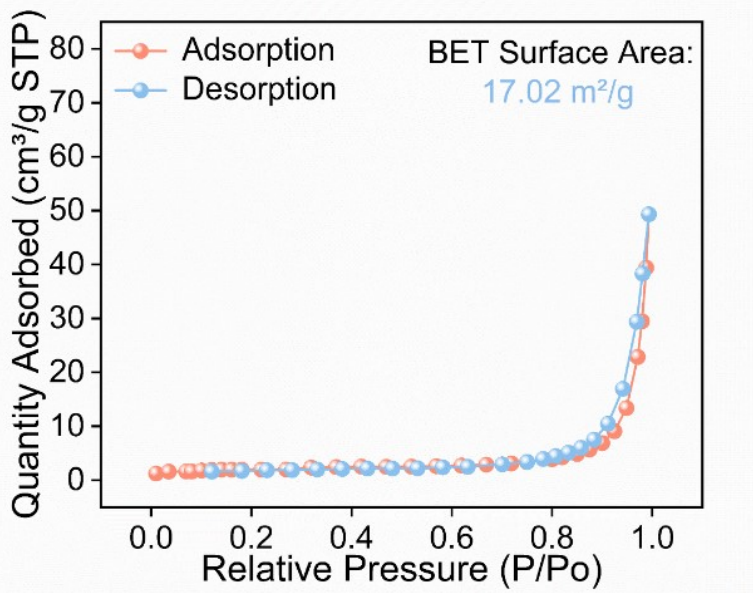

Fig. S11. N_2 adsorption/desorption isotherm of $MoSe_2$.

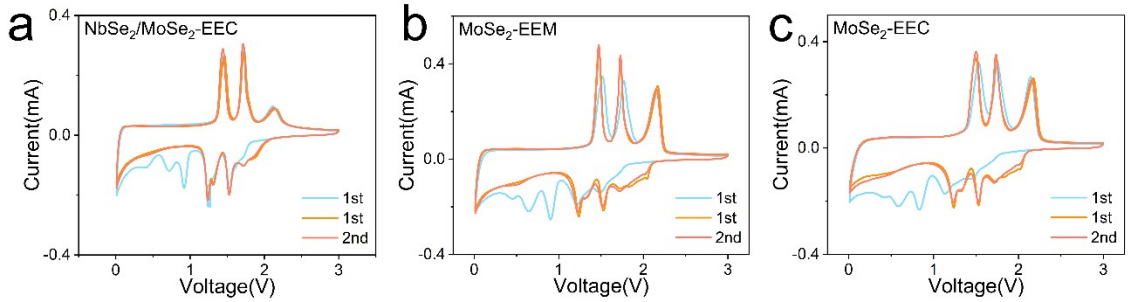

Fig. S12. CV curves for the first three laps of $NbSe_2/MoSe_2$-EEM(a)、$MoSe_2$-EEM(b) and $MoSe_2$-EEC(c).

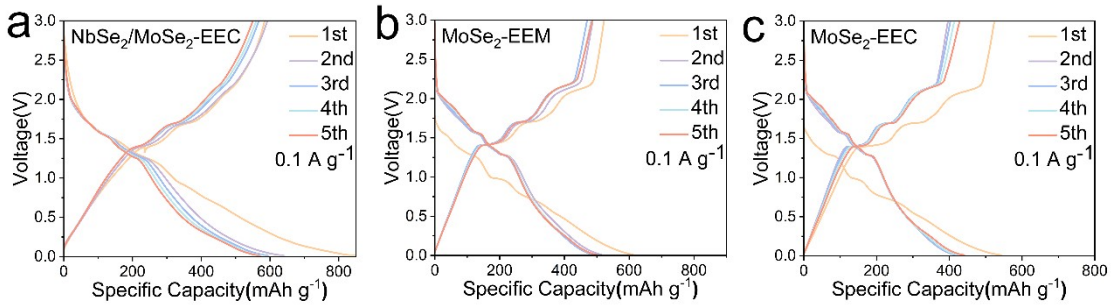

Fig. S13. Voltage-specific capacity curve for the first five turns of $NbSe_2/MoSe_2$-EEC(a)、$MoSe_2$-EEM(b) and $MoSe_2$-EEC(c).

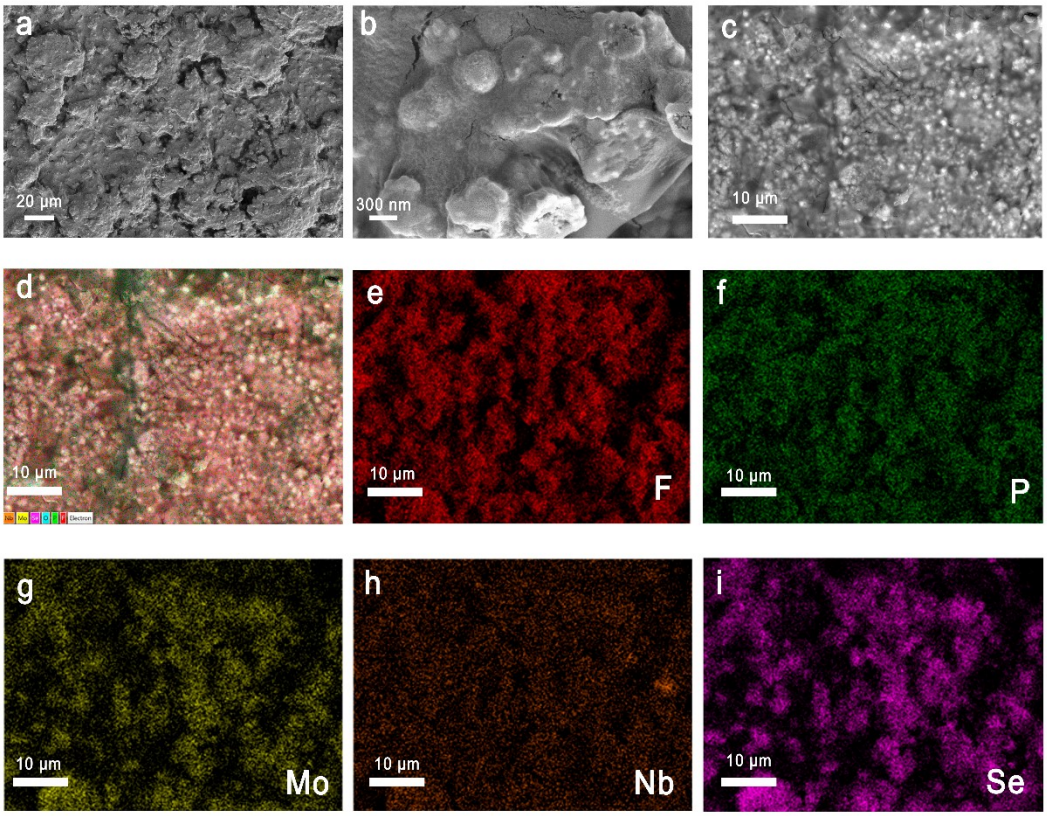

Fig S14 Morphology after 20 cycles (a, b), EDS images (c), and elemental distribution(d-i).

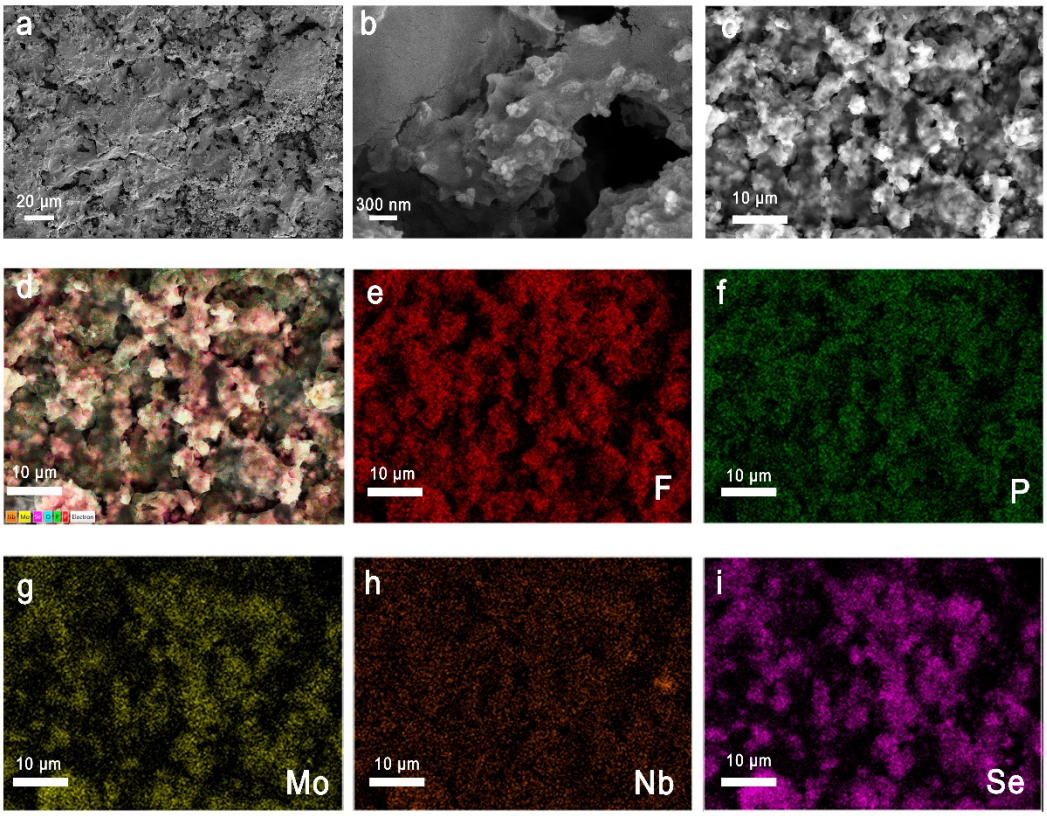

Fig. S15 Morphology after 50 cycles (a, b), EDS images (c), and elemental distribution(d-i).

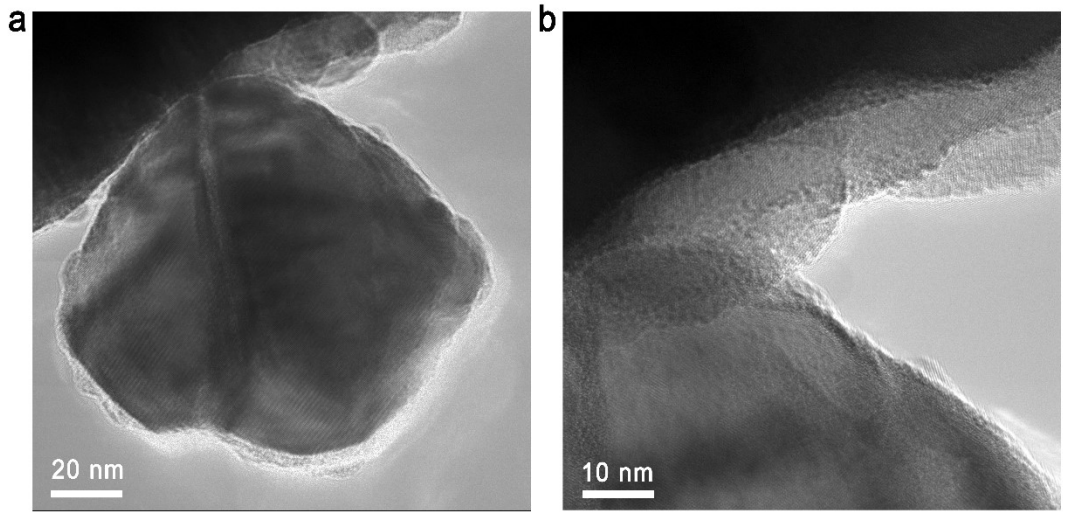

Fig. S16 TEM images of the $NbSe_2/MoSe_2$ electrode after cycling.

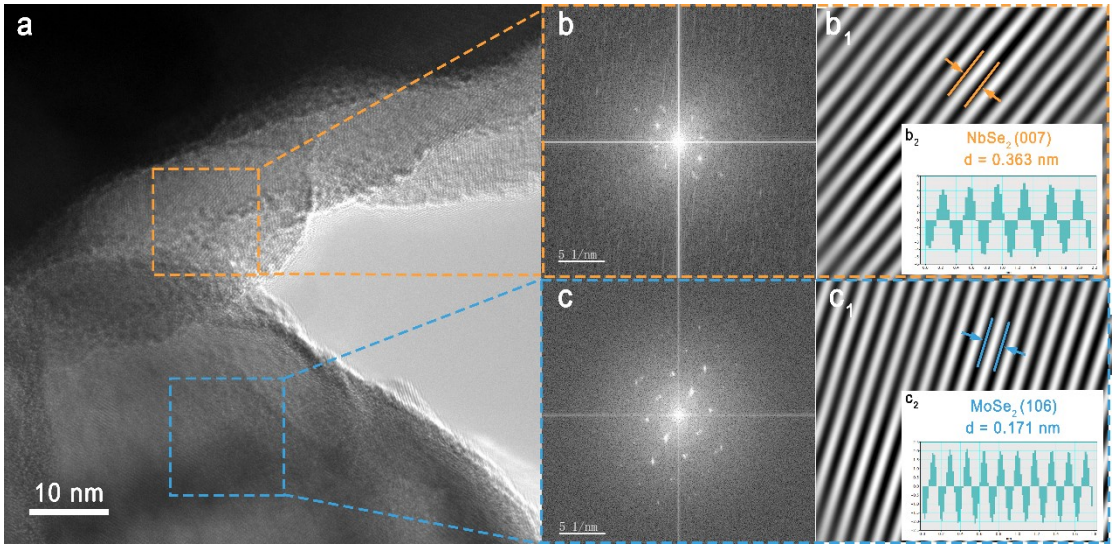

Fig. S17 Heterointerface (a), FFT (b, c), and lattice fringe analysis of the $NbSe_2/MoSe_2$ electrode after cycling (b1, b2, c1 and c2).

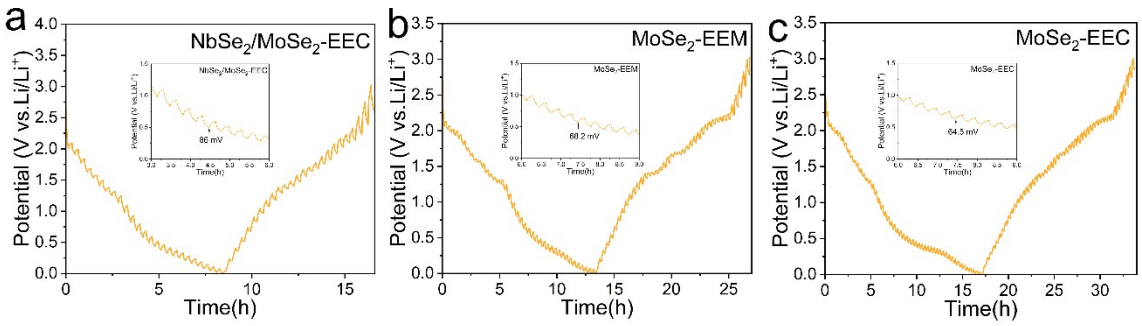

Fig. S18. GITT profiles of (a) $NbSe_2/MoSe_2$-EEC, (b) $MoSe_2$-EEM and (c) $MoSe_2$-EEC.

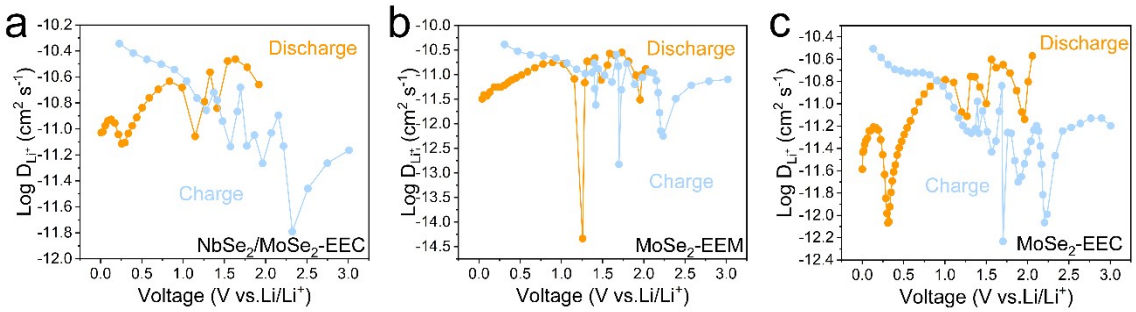

Fig. S19. Diffusion coefficient of Li^+ for $NbSe_2/MoSe_2$-EEC(a)、$MoSe_2$-EEM(b) and $MoSe_2$-EEC(c).

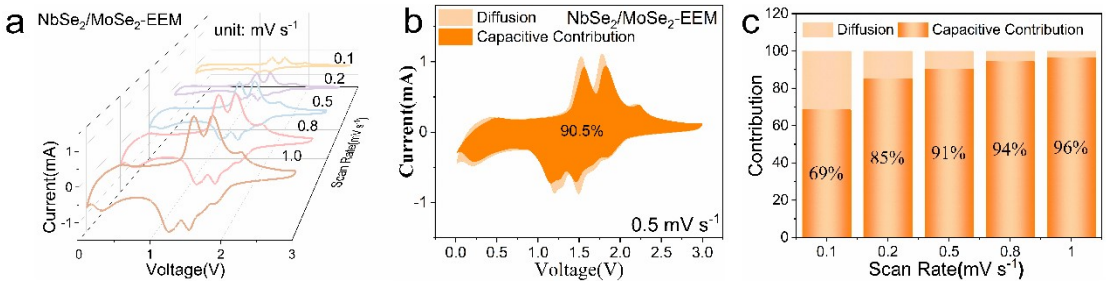

Fig. S20 (a) CV curve of $NbSe_2/MoSe_2$-EEM at different scanning speeds. (b) The pseudocapacitive contribution of the electrode at 0.5 mV s^{-1}. (c) pseudocapacitance ratio of $NbSe_2/MoSe_2$-EEM at different scanning speeds.

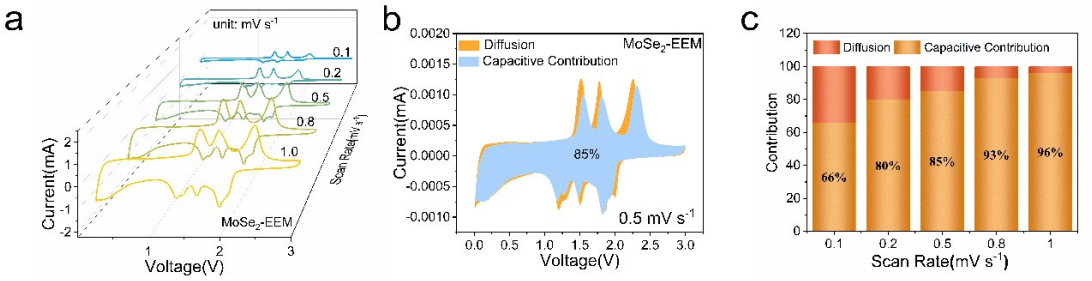

Fig. S21 (a) CV curve of $MoSe_2$-EEM at different scanning speeds. (b) The pseudocapacitive contribution of the electrode at 0.5 mV s-1. (c) pseudocapacitance ratio of $MoSe_2$-EEM at different scanning speeds.

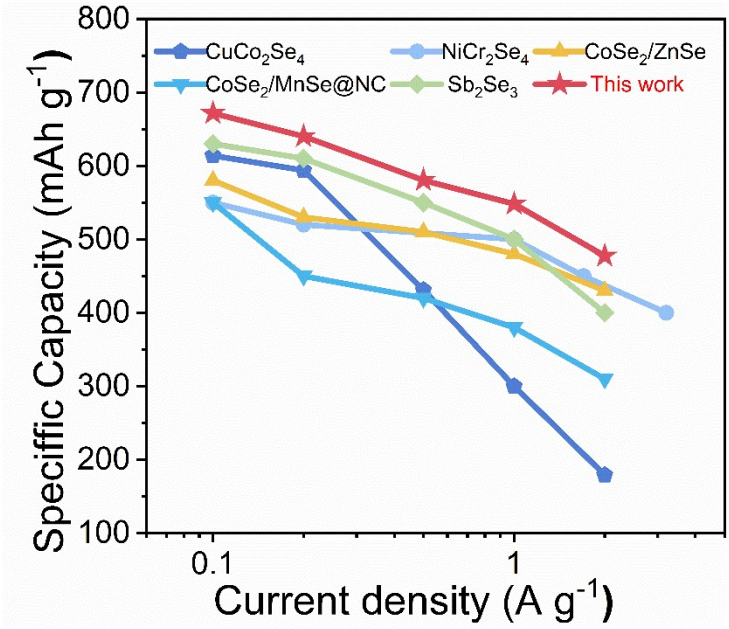

Fig. S22 (a) Half cell performance comparison of the $NbSe_2/MoSe_2$ anode with other reported anodes.

1

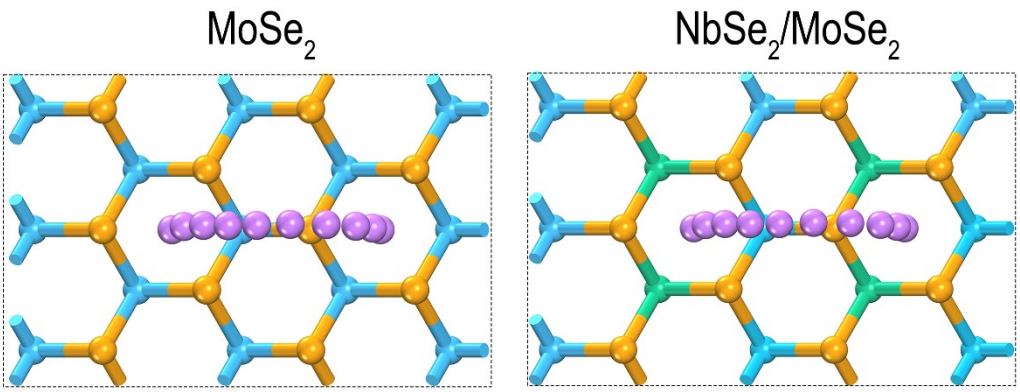

2

3 Fig S23 The Li^+ migration pathways corresponding to $MoSe_2$ and $NbSe_2/MoSe_2$.

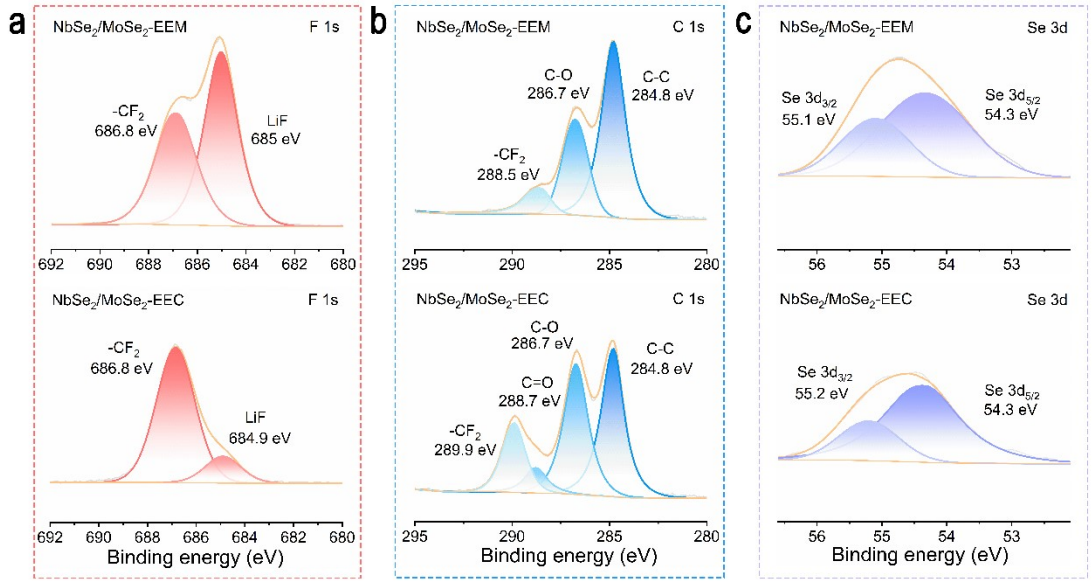

Fig. S24 F, C, and Se fine XPS spectra of $NbSe_2/MoSe_2$-EEM and $NbSe_2/MoSe_2$-EEC.

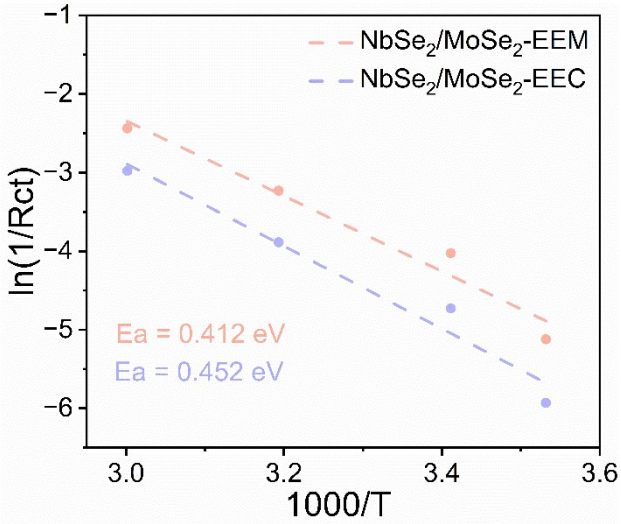

Fig. S25 Activation energy of $NbSe_2/MoSe_2$ in different systems.